Microchim Acta
https://doi.org/10.1007/s00604-019-3636-x

ORIGINAL PAPER

Integration of microbead DNA handling with optomagnetic detection in rolling circle amplification assays

Gabriel Antonio S. Minero[1] · Valentina Cangiano[1] · Francesca Garbarino[1] · Jeppe Fock[2] · Mikkel Fougt Hansen[1]

Received: 19 February 2019 / Accepted: 25 June 2019

Abstract

Rolling circle amplification (RCA) is a linear isothermal amplification technique that is widely applied in biomolecular assays due to its high specificity. Handling of a target sample using magnetic microbeads (MMBs) in a multi-step assay is appealing as the MMBs enable separation and transportation using an external magnet. Detection of amplicons using optomagnetic measurements of the rotational diffusion properties of magnetic nanoparticles (MNPs) is also appealing as it can be performed on any transparent sample container. Two strategies are described for integration of MMB sample handling in an RCA assay with on-chip optomagnetic detection of the amplification products. The first strategy relies on selective and irreversible release of the amplicons from the MMBs so that the binding of functionalized MNPs to the amplicons can be detected optomagnetically. The second strategy relies on the incorporation of MNPs into RCA products during RCA, followed by their separation on MMBs and subsequent optomagnetic detection upon release from the RCA products. Using MMB handling of RCA steps, the limits of detection (LODs) for a synthetic DNA target representative of Victoria Influenza type B were found to be between 4 and 20 pM with total assay times between 2 and 2.5 h. Without magnetic microbead sample handling, the LOD was 200 fM. The findings provide deeper insight into the use of magnetic microbeads as solid substrates to handle a DNA target for integration of RCA as well as other DNA-based assays.

Keywords Biosensor · Assay integration · DNA capture · DNA melting · Magnetic microbead

Introduction

Isothermal amplification of nucleic acid targets is attractive for fast and simple molecular detection of pathogens at an early stage. A great variety of techniques with exponential or linear amplification over time have been proposed [1]. Among these techniques is rolling circle amplification (RCA) [2]. In RCA, a circular template is formed by annealing and ligation of a padlock probe (PLP) onto the target. The 3′-end of DNA targets, hybridized on the circularized PLPs, is extended by the phi29 polymerase, which displaces newly synthesized DNA to continue the rolling circle amplification. This leads to formation of a long single-stranded DNA concatemer containing repeated copies of the DNA sequence complementary to the PLP. Typically, 1000 copies of the approximately 100 nt long PLP are produced in 1 h. RCA takes place at 30-40 °C and due to the high processivity of the phi29 polymerase, linear amplification can continue for up to 20 h. Compared to exponential isothermal amplification methods, RCA is slower but has several features that are advantageous for biosensing applications: First, the PLP recognition step is highly specific and can be sensitive to single point mutations with up to 100% specificity [3]. Second, the assay does not require reverse transcription of an RNA target and can also be tailored to detect other biomarkers than nucleic

The work was supported by DFF project (#4184-00121B). VC thanks Erasmus+ Program (Key action 1 A.Y. 2017-18) and Roberto Raiteri for sponsoring of the Erasmus program. JF acknowledges MUDP for support (MST-141-01415).

Electronic supplementary material The online version of this article (https://doi.org/10.1007/s00604-019-3636-x) contains supplementary material, which is available to authorized users.

✉ Gabriel Antonio S. Minero
gant@dtu.dk

✉ Mikkel Fougt Hansen
mfha@dtu.dk

[1] Department of Health Technology, Technical University of Denmark, DTU Health Tech, Building 345C, DK-2800 Kongens Lyngby, Denmark

[2] Blusense Diagnostics ApS, Fruebjergvej 3, DK-2100 Copenhagen, Denmark

Published online: 11 July 2019

acids [4]. Third, the amplification product is single stranded, which simplifies detection in hybridization-based readout schemes.

RCA products (RCPs) are coils of DNA with a size of 0.2-1 μm after about 30-60 min of RCA. The coils can be labelled with fluorescent tags and visualized using fluorescence microscopy [5]. The fluorescence of molecular beacons has been used to detect RCP concentrations from 10 pM to 10 nM where the results also revealed a strong sensitivity to intra- as well as inter-molecular loops in the RCPs that caused self-quenching of the beacons [6]. Furthermore RCPs were directly visualized using confocal microscopy with a limit of detection (LOD) falling between 3 and 30 fM [7]. The Nilsson group demonstrated discrimination and quantification of individual RCPs by a mobile-phone-based microscope over a 4-log dynamic range (1 fM to 10 pM) after an RCA time of 3 h [8].

The RCPs provide a dose-dependent readout upon hybridization to capture sequences, for example grafted onto micro- or nanoparticles. The binding of functionalized magnetic nanoparticles (MNPs) to RCPs has been detected via the resulting change in the hydrodynamic size of the MNPs using magnetic susceptibility or optomagnetic measurements with LODs of 10 pM for 1 h of RCA [9, 10]. Alternatively, the RCPs can be cleaved into monomers (the repeating unit complementary to the PLP) using a restriction enzyme. The monomers are then used to link two populations of functionalized nanoparticles to obtain a more sensitive readout. A monomer LOD of 30 pM was demonstrated using an optomagnetic readout with a detection time that was reduced to 7 min by use of magnetic incubation [11]. This monomer LOD corresponds to a predicted RCP detection LOD of about 30 fM for 1 h of RCA. Using gold nanoparticles and a colorimetric readout, a target LOD of 70 fM was obtained after 2 h of RCA [12].

Magnetic microbeads (MMBs) have proven highly useful as a solid substrate for multi-step sample processing in automated laboratory equipment as well as in microfluidic systems [13–17]. They can be simply manipulated using an external magnet and it is therefore attractive to implement them in a complete multi-step RCA assay, for example, in multi-round circle-to-circle RCA (C2CA). In C2CA, a step of particular importance is the separation of unreacted PLPs from PLPs ligated onto targets. The PLPs remaining from the previous ligation will otherwise interfere with re-circularization of monomers made of the complementary sequence. This step has usually been achieved using MMBs functionalized to capture the target with attached RCPs [4, 18]. Although there are advantages of bead-based multi-step nucleic acid processing, the MMBs may interfere with enzymatic amplification [19] and potentially also the detection [20, 21]. Some work has been undertaken to further integrate RCA on an automated platform [22–25], but there is still a need for automation of the RCA processing and integration with detection [15].

Here, we investigate integration strategies for the multi-step RCA assay comprising (1) DNA ligation and capture on MMBs, (2) RCA performed on MMBs, and (3) on-chip optomagnetic (OM) readout of the RCPs. To combine the controlled release of targets from MMBs with binding of functionalized MNPs during detection, we use real-time OM measurements vs. temperature to characterize the properties of the involved DNA hybrids. We present and demonstrate a strategy for the robust capture and microbead DNA handling during RCA combined with a selective and irreversible release of intact amplicons and their simultaneous detection (Strategy I). We also present and demonstrate an alternative readout strategy where MNPs are trapped in RCA products on microbeads and subsequently released for detection in a high-pH buffer (Strategy II). These strategies are compared to reference experiments without MMB handling where the OM detection is performed on RCPs directly mixed with functionalized MNPs.

Experimental

Reagents, buffers and DNA sequences

Ampligase, BSA, dNTP mix and Ligation buffer (10×) (200 mM Tris-HCl, 250 mM KCl, 100 mM $MgCl_2$, 5 mM NAD, 0.1% Triton X-100, pH 8.3) were purchased from Nordic Biolabs (www.nordicbiolabs.dk). Phi29 polymerase and RCA buffer (10×) (330 mM Tris-CH_3COOH, 100 mM $Mg(CH_3COO)_2$, 660 mM K-CH_3COOH, 1.0% Tween 20, 10 mM DTT, pH 7.9) were purchased from Thermo Fischer (www.thermofisher.com).

Additionally, the following buffers were used (reagents from Sigma-Aldrich, www.sigmaaldrich.com): Binding buffer (1×): 8 mM tris, 4 mM EDTA, 0.1 Tween-20, and 0.8 M NaCl (pH 8); pH 8/12 detection buffer (1×): 20 mM Tris-HCL, 140 mM NaCl, 5 mM KCl, 50 mM EDTA, 0.1% BSA, 0.01% Tween20, pH adjusted to 8 using HCl or to 12 using NaOH.

Bionized NanoFerrite (BNF) starch streptavidin magnetic nanoparticles with a nominal diameter of 100 nm were purchased from Micromod Partikeltechnologie GmbH (www.micromod.de, prod. code 10-19-102).

MyOne Streptavidin C1 magnetic microbeads with a nominal diameter of 1 μm were purchased from Thermo Fisher (www.thermofisher.com).

The padlock probe was designed to match a synthetic DNA target containing the hemagglutinin gene of Victoria, a type-B influenza virus strain as described previously [18]. The magnetic MMBs were functionalized with a 15 nt

capture oligo (CO) targeting a section of the target outside the binding region of the PLP. To perform the detection, MNPs were functionalized with a 20 nt detection oligo (DO) identical to a section of the user-chosen region on the non-target specific backbone of the PLP. The DNA sequences are given in the ESM, Table S1.

Functionalization of particles

To functionalize MNPs, 10 μL stock MNP solution (10 mg mL^{-1}) was mixed with 8 μL DO (1 μM) and 82 μL binding buffer (1×) to obtain a final volume of 100 μL. After incubation for 30 min at room temperature to allow the DO probes to bind to the MNPs, the MNPs were washed 3 times and resuspended in 100 μL pH 8 detection buffer (1×) to a concentration of 1 mg mL^{-1}.

MMBs were functionalized with biotinylated CO-probes that were complementary to the non-amplified part of the DNA target as follows: 36 μL stock MMBs (10 mg mL^{-1}) was mixed with 90 μL CO (1 μM) and 174 μL binding buffer (1×). After 30 min incubation at room temperature with end-over-end mixing, the MMBs were washed 3 times in binding buffer (1×) and finally resuspended in 300 μL ligation buffer (1×) with 0.2 mg mL^{-1} BSA to a concentration of 1.2 mg mL^{-1}.

RCA assay without microbead sample handling

Three stock solutions of target DNA with concentrations of 2 nM, 200 pM and 20 pM with addition of 3-fold excess of PLP were prepared in the ligation buffer (1×) with 0.2 mg mL^{-1} BSA and 250 u mL^{-1} ampligase. Sequence-specific annealing and PLP ligation was performed for 20 min at 55 °C.

50 μL of each of the three ligated target-PLP stocks was mixed with 25.3 μL milliQ water, 10 μL RCA buffer (10×), 10 μL BSA (2 mg mL^{-1}), 1.12 μL dNTP (10 mM), and 3.6 μL phi29 polymerase (10 u μL^{-1}) to obtain final volume 100 μL. A no template control (NTC) was prepared in the same manner with 50 μL of milliQ water instead of DNA. Tubes with the solutions were placed in a thermoblock at 38 °C. RCA was run for 45 min and terminated by heat inactivation of the phi29 polymerase for 10 min at 65 °C.

Different volumes of the three RCP stocks were mixed with DO-MNPs in pH 8 detection buffer (1×) to obtain a final MNP concentration of 0.05 mg mL^{-1} and final target-PLP concentrations c [pM] of 200, 40, 30, 20, 10, 4, 2, 1, 0.4, 0.2, and 0. The samples were subsequently mounted in chips in the OM setup pre-heated to 54 °C and OM measurements were initiated.

RCA assays with microbead sample handling

A schematic of the two strategies with microbead sample handling is given in Fig. 1.

The 2 nM and 200 pM DNA targets with ligated PLPs were prepared as described in the previous Section. The DNA hybrids were further diluted in ligation buffer (1×) with 0.2 mg mL^{-1} BSA and mixed with CO-functionalized MMBs (CO-MMBs) to obtain a 100 μL sample. The final

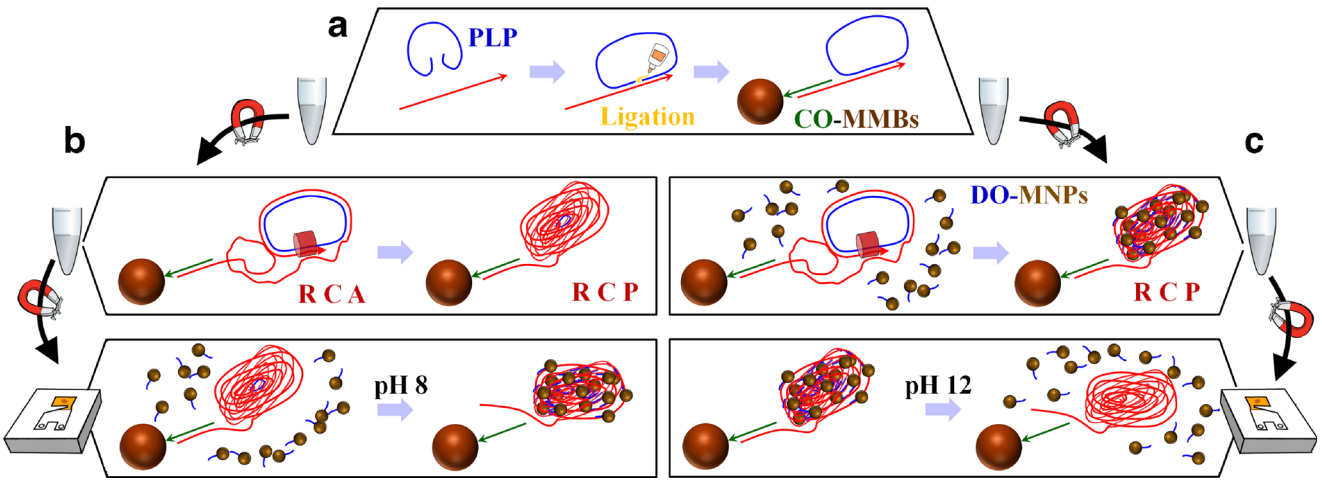

Fig. 1 Schematic of the two assay strategies with microbead sample handling. **a** The assays share the ligation step (20 min at 55 °C) as well as the capture of DNA target on MMBs (3 min at 55 °C, 30 min cooling down to ≈ 35 °C, and 30 min at ≈ 23 °C). The following steps are RCA (45 min at 38 °C) and OM detection. **b** In Strategy I, the DO-MNPs are added to the detection buffer in which the RCP-MMB complexes are suspended after RCA. RCPs are released from MMBs and the binding of DO-MNPs is detected (20 min at 54 °C). **c** In Strategy II, DO-MNPs are incorporated in RCPs during RCA and their subsequent release in the high-pH detection buffer is monitored (3 min at 38 °C). The schematic indicates when the MMBs are magnetically separated (≈ 1 min) and whether the reaction step takes place in a tube or in a chip. Prior to OM detection of MNPs in suspension, the MMBs were dragged to the bottom of the chip to form a diffuse pellet. Four samples were processed simultaneously

DNA target concentrations ranged from 2 pM to 200 pM and the final MMB concentrations was either 0.1 mg mL^{-1} or 0.3 mg mL^{-1}. For the NTC, no DNA was added.

To maximize the efficiency of the capture of target-PLPs on CO-MMBs, we used the following two-step mixing procedure: (1) heating of target-PLP hybrids and MMBs to 55 °C for 3 min followed by ramping of the temperature to ≈ 35 °C over 30 min under constant rotation mixing at 1000 rpm in a thermoshaker; (2) end-over-end mixing at room temperature for 30 min. Four tubes were processed simultaneously. By ramping up the temperature formation of unwanted secondary structures and dimers was avoided [26]. Subsequently, the CO-MMBs with attached target-PLPs were separated magnetically from unreacted PLPs (Fig. 1a) using a home-built high-gradient magnetic separator consisting of a tube holder and an array of permanent magnets. In this separator, the MMBs were captured on the tube wall in a matter of seconds.

In Strategy I with detection of MNP binding to RCPs (Fig. 1b), the resulting MMB pellet was gently resuspended in 20 μL RCA buffer (10×), 2.25 μL dNTP mix (10 mM), 20 μL BSA (2 mg mL^{-1}), 3.6 μL phi29 polymerase (10 u μL^{-1}), and 54.2 μL milliQ water and RCA was performed in a thermoshaker at 38 °C and 1000 rpm. The rotation mixing at 1000 rpm was used to prevent sedimentation of the MMBs, which would be detrimental for the results. The mixing was found to somewhat reduce the efficiency of the phi29 polymerase (ESM, Section S2). The amounts of added phi29 buffer, BSA, and dNTPs were doubled to improve diffusion of reagents to the MMBs, whereas the concentration of phi29 polymerase was kept same as in Section "RCA assay without microbead sample handling". After 45 min of RCA, the MMBs were again magnetically separated, transferred into 100 μL of pH 8 detection buffer (1×) with 0.05 mg mL^{-1} DO-MNPs and injected into a chip for OM characterization.

Strategy II, with detection of MNP release from RCPs (Fig. 1c), followed the same procedure for RCA, except that 5 μL of milliQ water was replaced with 5 μL of DO-functionalized MNPs (1 mg mL^{-1}). During RCA, DO-MNPs were captured on RCPs bound to the MMBs. After RCA, a gentle magnetic separation was performed to separate DO-MNPs bound to RCPs from free DO-MNPs. This separation was performed for 1 min in a home-built low-gradient magnetic separator consisting of a tube holder and an array of permanent magnets with a larger spacing to the tubes. In this, the MMB-RCP-MNP complexes were captured in tens of seconds whereas free MNPs remained in suspension. Subsequently the MMB-RCP-MNP complexes were washed in pH 8 detection buffer (1×) to remove DO-MNPs that were not bound to RCPs. After magnetic separation, the MMB-RCP-MNP conjugates were resuspended in 100 μL of pH 12 detection buffer (1×) and injected into a chip for OM detection. The high-pH buffer denatured the DNA hybrids and released the MNPs from the MMB-RCP-MNP complexes and the OM signal from free MNPs was detected.

Optomagnetic measurements

The OM setup, made for parallel detection of four assays in disposable plastic chips, was described previously in Minero et al. [27]. In brief, each chip was placed between two custom-made heaters with a temperature controlled using a Stanford Research Systems PTC10 unit (www.thinksrs.com) and monitored using Pt100 elements. Light (wavelength of 405 nm) was guided from a light emitting diode to the side of the chip, and from the other side of the chip to a photodetector (Thorlabs PDA-36A-EC, www.thorlabs.com). The optical path length within the detection chamber of the chip was 5 mm. A sinusoidal homogeneous magnetic field of amplitude 1 mT in the detection chamber was produced by two coils supplied by a custom-built voltage-to-current converter controlled by a National Instruments (www.ni.com) USB-6341 data acquisition card, which also collected the photodetector signals. Measurements of OM spectra comprising 41 logarithmically spaced frequencies between $f = 1$ and 2800 Hz were initiated immediately after temperature equilibration of the chip in the pre-heated setup (≈1 min) and allowed to continue with one spectrum every 45 s for up to 100 sweeps (≈ 75 min).

Before a chip was mounted in the OM setup in protocols with microbead sample handling, the MMBs were captured at the bottom of the chip detection chamber to a diffuse pancake-like pellet using an external magnet to avoid interference of the MMBs with the subsequent OM measurements of the MNPs.

The OM technique measures the modulation of the intensity of light transmitted through the MNP suspension in response to a magnetic field applied along the light path as a function of the frequency f of the magnetic field. The ability of the MNPs to rotate in response to the applied field depends on their hydrodynamic size such that smaller MNPs can follow the field up to higher f than large MNPs. For a magnetic field excitation of $B(t) = B_0 \sin(2\pi f t)$ we have previously shown that the real 2nd harmonic photodetector voltage (indicating the $\sin(4\pi f t)$-component of the signal) normalized by 0th harmonic voltage, V_2'/V_0, shows a characteristic peak at

$$f_p \approx 0.7 f_B = 0.7 \frac{k_B T}{\pi^2 \eta D_h} \quad (1)$$

Here f_B is the Brownian relaxation frequency, $k_B T$ is the thermal energy, η is the viscosity and D_h is the average hydrodynamic diameter of the MNPs [28]. When MNPs bind to RCPs, their size increases substantially from that of the free MNPs ($\approx$ 100 nm). The signal at high frequencies can therefore be used to quantify the amount of free MNPs for a given target concentration. Here, we detect RCPs as a 'turn-off' signal detecting the depletion of free MNPs as they bind to the RCPs or as a 'turn-on' signal when MNPs are released from RCPs.

Results

In this section, we present the results of a reference OM detection assay performed without MMB sample handling and subsequently the results obtained for the assays with MMB handling. We compare detection of the 'turn-off' signal from MNPs when they bind to the RCPs (Strategy I) and of the 'turn-on' signal from MNPs when they are released from being captured in RCPs (Strategy II).

All experiments were carried out with a combined PLP annealing and ligation at 55 °C for 20 min and RCA at 38 °C for 45 min. The OM spectra were obtained as a function of time (one spectrum every 45 s). Error bars indicate the sample standard deviation (SD) obtained from triplicate or quadruplicate experiments. The LOD was estimated from the NTC signal plus three SD. Dose-response curves, $f(c)$ vs. DNA target concentration c, were analyzed in terms of the Hill equation, $f(c) = f(0) + [f(\infty) - f(0)] / \left[1 + (K_A/c)^{n_H}\right]$, where K_A is the association constant and n_H is the Hill coefficient. The Hill coefficient indicates the cooperativity of the binding, where $n_H \approx 1$ indicates non-cooperative binding and $n_H > 1$ indicates cooperative binding.

RCA assay without microbead sample handling

In these reference experiments, DO-functionalized MNPs were spiked directly into the solutions of RCPs after RCA. Compared to previous studies [9, 29–31], the detection buffer and temperature were optimized by addition of EDTA and using an elevated detection temperature to minimize self-annealing of the RCPs. Furthermore, during detection the depletion of MNPs due to binding to RCPs was monitored in real time at 54 °C rather than at the end-point at room temperature.

Figure 2a shows OM spectra measured for samples with target concentrations of $c = 0$ pM (NTC), 10 pM, and 40 pM approximately 20 min after initiation of detection. The spectra show a negative peak at frequencies near 200 Hz, which is attributed to free MNPs, and features below about 10 Hz, which are attributed to MNPs bound to RCPs. We detected the binding of MNPs to the RCPs via the depletion of the signal from free MNPs. As a measure of the signal from free MNPs in spectrum number n, we took the average normalized signal

$$\langle V_2'/V_0\rangle(n) \equiv N^{-1} \sum_f V_2'(f,n)/V_0(f,n), \tag{2}$$

where the sum was taken over N frequencies between 40 Hz and 1 kHz indicated by the vertical dashed lines in Fig. 2a. Taking the initial amount of free MNPs as that measured in the first spectrum obtained after temperature equilibration of the chip, we define the fractions F_{MNP} and B_{MNP} of free and bound MNPs, respectively, in the n'th spectrum in a series of measurements as

$$F_{MNP} = 1 - B_{MNP} = \langle V_2'/V_0\rangle(n)/\langle V_2'/V_0\rangle(1). \tag{3}$$

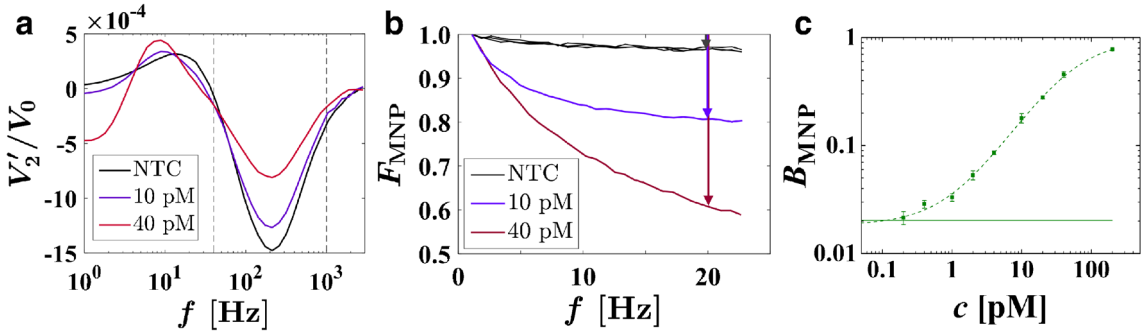

Fig. 2 Detection of MNP binding to RCPs without microbead sample handling (reference). The functionalized MNPs were mixed directly with RCPs after 45 min of RCA for the indicated target concentrations, c, and OM spectra were measured as function of time at 54 °C. **a** OM spectra measured 20 min after mixing. The vertical dashed lines indicate the frequency windows used to quantify the signal from free MNPs. **b** Time evolution of the fraction of free MNPs, F_{MNP}, in the n'th spectrum during OM detection (45 s per spectrum). **c** Fraction of MNPs bound to RCPs after 20 min, B_{MNP}, vs. c obtained from quadruplicate experiments. The horizontal line indicates the signal cut-off (NTC signal+3×SD). The dashed line is a Hill equation fit with $K_A = 48$ pM and $n_H = 1.0$

Figure 2b shows F_{MNP} vs. time for the indicated target concentrations. It is observed that a higher target concentration led to a lower signal from free MNPs as more MNPs were bound to RCPs, and that as time progressed more MNPs were bound to RCPs. For the NTC sample, F_{MNP} was found to decrease by about 2% due to unspecific interactions. Inspecting Fig. 2b, we observe that the signal for $c = 10$ pM was close to saturation after about 20 min ($n = 27$). As a compromise between signal and speed of measurement, we therefore chose to use this time for the quantification. Figure 2c reports the fraction of bound MNPs after 20 min of detection as function of the target concentration c. The NTC had a signal $B_{MNP}\pm$ SD=0.0182±0.0007. From the dose-response curve, we found an LOD of 200 fM. From the Hill model fit, we found a Hill coefficient of $n_H = 1.0$, which suggests that the binding of MNPs to RCPs is non-cooperative.

Microbead sample handling with detection of MNP-binding to RCPs (Strategy I)

In Strategy I the DNA target was captured on CO-functionalized MMBs, which were used as a handle to transport the DNA target complex through amplification to OM detection (Fig. 1b). To perform the multi-step processing of DNA using MMBs, the capture oligo (CO)-target hybrid should be stable at the reaction conditions used for ligation and RCA. Furthermore, to reduce diffusion limitations, the RCPs should be released from the MMBs in the detection step. Under the same conditions, the detection oligo (DO)-RCP hybrids should be stable to enable 'turn-off' detection of the binding of CO-functionalized MNPs to RCPs. We therefore characterized the melting of CO-target hybrids for the CO sequence, which was chosen to have a 15 nt sequence matching the target (ESM, Table S1).

For the melting assays, RCPs (45 min of RCA) were grown on target-PLPs that were pre-attached to MNPs. Subsequently, real-time OM measurements were performed at temperatures increasing at 0.01 °C s^{-1}. The hydrodynamic MNP size D_h vs. temperature was extracted from the peak position in the V_2'/V_0 spectra using Eq. 1 [27] and is shown in Fig. 3.

The melting profiles were found to be reproducible and indicated that D_h decreased to the value for the free MNPs when the temperature exceeded a characteristic melting temperature T_m estimated as the midpoint between the initial and final D_h-values. For the CO-target hybrids we estimated $T_m \approx 54$ °C. We note that this temperature is close to the temperature used for ligation (55 °C) and well above the RCA temperature (38 °C). The DO-labelled curves in Fig. 3 reveal a more abrupt decrease in D_h corresponding to a melting temperature of $T_m \approx 71$ °C. The well-defined temperature transitions observed for the

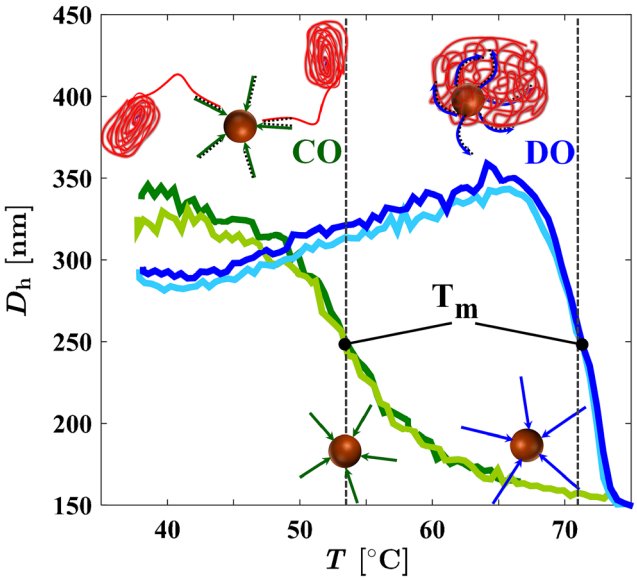

Fig. 3 Melting profiles measured for the capture and detection oligonucleotides on MNPs. Hydrodynamic diameter D_h vs. temperature calculated from peaks of OM spectra in two repeated experiments on individual MNPs with attached RCPs as illustrated in top panel. In CO experiments, RCPs were grown on targets captured on CO-functionalized MNPs. In DO experiments, DO-functionalized MNPs were saturated with RCPs. The melting temperatures, Tm, corresponding to the release of RCPs from the MNPs, are indicated

two cases show that the size change is due to specific DNA interactions. The difference in the slopes of the melting curves is attributed to stronger hybridization cooperativity of DOs than COs; the CO has only one binding site on an RCP, whereas the DO has many binding sites on an RCP (one for each repeated copy of the PLP). Therefore, DO-MNPs can have many simultaneous bonds to a single RCP, which increases the melting temperature and makes the transition occur over a narrower temperature interval. Once the RCPs were formed, the release of the target from the CO was essentially irreversible with virtually no recapture as the single target sequence was buried within the DNA cloud of the RCP. In contrast, the release of the RCPs from the DO-functionalized MNPs was found to be partly reversible (ESM, Section S3).

Subsequently the CO-functionalized MMBs were used as movable support for targets with pre-ligated PLPs during (1) target capture, (2) RCA, and (3) release of RCPs from MMBs with simultaneous detection of the DO-functionalized MNPs bound to the RCPs (Fig. 1b). In these studies, the importance of the MMB concentration was investigated as it can potentially impact the assay performance.

Detection was performed at 54 °C, which was found to be the optimal temperature in the range between 52-56 °C (ESM, Section S4). This temperature is the melting temperature of the CO-target hybrids and well below the

melting temperature of the DO-RCP hybrids (Fig. 3). This choice of temperature also allowed for a direct comparison of Strategy I to the MMB-free reference assay, which was performed using the same detection temperature. The OM spectra (ESM, Section S4) had features similar to those shown for the MMB-free strategy in Fig. 2a and b, and we therefore analyzed the free MNP turn-off signal, B_{MNP}, using the same approach. For the calculation of B_{MNP}, a 20 min detection time was used as in the reference assay. Prolonging detection time up to 75 min did not improve the LOD.

Figure 4a shows B_{MNP} vs. c for the two investigated MMB concentrations c_{MMB} of 0.1 mg mL^{-1} and 0.3 mg mL^{-1}. From Hill model fits, we found n_H-values of 1.3 and 2.5 for the two MMB concentrations, respectively. The observed increase of the Hill coefficient indicates higher cooperativity of the hybridization between RCPs and COs (on MMBs) for higher CO-MMB concentration. This is likely due to the excess of free CO probes near the RCPs in the MMB pellet. For c_{MMB}=0.1 mg mL^{-1} and 0.3 mg mL^{-1}, respectively, we found NTC signals $B_{MNP}\pm$ SD=−0.030 ± 0.014 and 0.000±0.017 and LODs of 4 pM and 20 pM.

To verify that RCPs were indeed released from MMBs during detection and that DO-functionalized MNPs bound specifically to the RCPs we further investigated selected samples (c[pM] = 40, 100, 160, and 200) after the detection step. First, the MMBs were selectively captured and removed using a magnetic separator with a low magnetic field gradient and the MMB-free supernatant was studied in a temperature melting experiment. This experiment revealed clusters of MNPs with signal features at frequencies below 40 Hz that underwent a melting transition to free MNPs at a temperature of about 72 °C (ESM, Section S5). This confirmed that the RCPs were released from the MMBs during the detection step and the sharpness as well as temperature of the transition confirmed that the binding of the MNPs to the RCPs was mediated by specific interactions.

Microbead sample handling with detection of MNP-release from RCPs (Strategy II)

In Strategy II the DNA target was captured on CO-functionalized MMBs, which were used as solid support for the target with pre-ligated PLPs during (1) target capture and (2) RCA in the presence of DO-functionalized MNPs. This was followed by magnetic separation of MMBs with attached RCP-MNP complexes and washing to remove unbound MNPs. Finally, (3) the MMB-RCP-MNP complexes were resuspended in a high-pH detection buffer (pH 12) and the turn-on signal from released free MNPs was detected (Fig. 1c). Except for the addition of DO-functionalized MNPs during RCA, all steps until detection

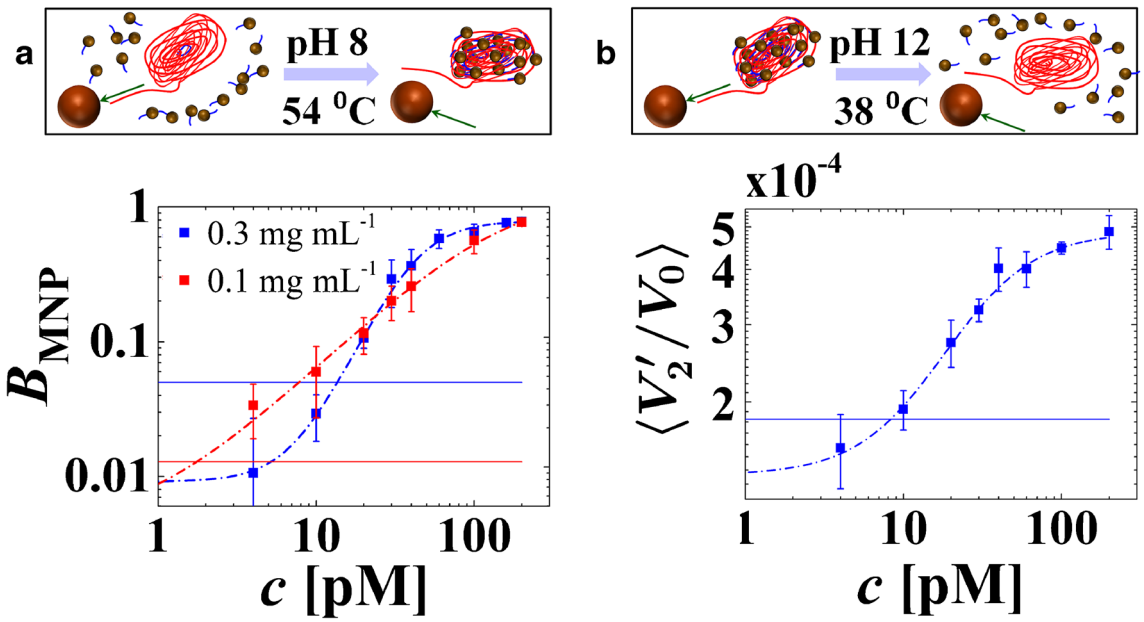

Fig. 4 Dose-response analysis of integrated RCA assay with two microbead sample handling strategies. **a** Strategy I - on-chip OM detection of the fraction B_{MNP} of MNPs bound to RCPs after 20 min of monitoring at 54 °C. Error bars indicate SDs (n = 4). Horizontal lines indicate signal cutoff (NTC+3×SD) and dashed lines are Hill equation fits with K_A = 74 pM and n_H = 1.3 (c_{MMB} = 0.1 mg mL^{-1}) and K_A = 42 pM and n_H = 2.5 (c_{MMB} = 0.3 mg mL^{-1}), respectively. **b** Strategy II - on-chip OM detection of MNP turn-on signal, $\langle V_2'/V_0\rangle$, upon release from RCPs in high-pH buffer after 2 min of monitoring at 38 °C. Error bars indicate SDs (n = 3). The horizontal line indicates the signal cutoff (NTC+3×SD) and the dashed line is a Hill equation fit with K_A = 27 pM and c_H = 1.7

in step (3) were carried out as described for Strategy I. Upon resuspension in the high-pH buffer, the DNA hybrids denatured [32] and the MNPs were released from the RCPs. As for Strategy I, the MMBs were captured at the chip bottom using a permanent magnet to minimize interference with the subsequent quantification of the released MNPs, which took place at 38 °C. To better enable visual verification of the capture of MMBs during magnetic separation from non-incorporated MNPs, all experiments were carried out for $c_{MMB} = 0.3\ mg\ mL^{-1}$. This protocol required only stability of the CO-target and DO-RCP hybrids until the final magnetic separation step.

The resulting OM spectra showed only features from free MNPs and MMBs with only a very weak signal from the NTC (ESM, Section S6). The signal from free MNPs reached a stable level within 2 min. In the dose-response analysis, we therefore considered the turn-on signal $\langle V_2'/V_0 \rangle$ from free MNPs measured after 2 min, which is shown as function of c in Fig. 4b. We found an NTC signal $B_{MNP} \pm$ SD$= (1.33 \pm 0.16) \times 10^{-4}$ and an LOD of 10 pM.

Discussion

Two new strategies to integrate optomagnetic detection with microbead sample handling in an RCA assay were presented and demonstrated. In Strategy I, the capture and detection probe sequences were tailored to allow for a selective and irreversible release of RCPs from MMBs to promote binding of functionalized MNPs to the RCPs. In Strategy II, MNPs captured on RCPs during RCA were detected upon their release at high pH. Both strategies share the fact that the conditions of the entire assay had to be optimized with the specific goal of integrating the sample handling and detection.

The reference assay without microbead sample handling showed an LOD of 200 fM for 45 min of RCA, which is significantly lower than previously reported values of 5 − 10 pM using OM or magnetic susceptibility readouts based on binding of functionalized MNPs to RCPs [9, 10]. The reduced LOD is likely due to that the detection took place in the presence of only 140 mM NaCl at constant $T = 54$ °C. In contrast to Strömberg et al. [9], we did not heat above T_m for the DO-RCP hybrids and we therefore avoided the signal loss arising from the need to re-capture DO-labelled MNPs on the RCPs.

The results also clearly indicate that the MMB handling reduced the assay performance as indicated by the comparison of the 200 fM LOD for the turn-off signal in the reference assay to the 4-20 pM LODs found in the assays with MMB handling. Comparing the B_{MNP} signal cut-offs, it is observed that the cut-offs for the MMB-free reference (Fig. 2c) and Strategy I with $c_{MBB} = 0.1\ mg\ mL^{-1}$ (Fig. 4a) assume nearly the same value, which is only about one third of the value found for Strategy I with $c_{MBB} = 0.3\ mg\ mL^{-1}$ (Fig. 4a). This is likely caused by the higher amount of MMBs in the measurement chamber interfering with the measurement on the MNP suspension. This interference can be of physical origin, for example if a variable amount of MMBs entered the light path through the chip or affected the MNPs magnetically in the applied measurement field. In addition, a higher amount of MMBs increased the probability to form short DO-CO hybrids, i.e. unspecific binding. This was primarily the cause of the signal variation in Strategy II due to a background from MNPs even in the NTC after washing (ESM, Section S6). Comparing the CO and DO sequences, we find that they form an overlap of three matching bases (ESM, Section S1), which due to cooperative binding of several DO-CO hybrids can produce an unspecific signal background. Consequently the NTC signal becomes more pronounced for a higher MMB concentration and a lower assay temperature. This hypothesis is supported by the observation of a significantly higher Hill coefficient n_H of 2.5 in Strategy I for $c_{MMB} = 0.3\ mg\ mL^{-1}$ compared to 1.3 for $c_{MMB} = 0.1\ mg\ mL^{-1}$ (Fig. 4a). Further investigations of this hypothesis and on how to reduce the effect of it will be topics of our future work.

The Hill coefficient n_H and the association constant K_A are used to compare the slopes and centre points of the dose-response curves. The results revealed dependence on both the assay strategy and the MMB concentration with a general shift of the dose-response curves to higher concentrations when MMB handling is used. A significant difference between the MMB-free assay and the MMB-using strategies is that all steps in the MMB-free reference strategy prior to detection take place in solution (homogeneous assay), whereas the amplification in the two latter strategies takes place on the MMB solid phase (heterogeneous assay). In the MMB-based strategies, the target is essentially immobile on the MMBs and the reaction rate is therefore to a higher degree limited by diffusion of the other reactants to the surface of the MMBs where the template concentration is potentially also high. The exchange of liquid between MMBs in an MMB pellet is limited. If the MMBs are not fully re-dispersed after magnetic separation, the output of the reaction will be reduced. Diffusion limitations can also reduce the signal in Strategy I and increase the time needed to reach a signal steady-state during the detection as RCPs released from the MMBs are initially at the bottom of the detection chamber. In contrast, the MNPs and RCPs were initially a homogeneous mixture in the MMB-free assay.

Finally, the activity of the phi29 polymerase may be affected by the presence of the MMBs [21] and by crowding due to other RCPs on the same MMB. In addition, to avoid sedimentation of the MMBs during the RCA reaction, it was performed in a thermoshaker at 1000 rpm. This vigorous mechanical agitation was found to reduce the polymerase activity (ESM, Section S2).

The use of MMBs and addition of magnetic separation steps increased the complexity of the presented strategies and made it more time and labor-consuming. However, the MMB handling also makes the assay protocol amenable to integration with automatic handling using external magnets, either in a robotic system or in a lab-on-a-chip device. Furthermore, the magnetic separation of target-PLP hybrids from the ligation solution with a potentially high concentration of unreacted PLPs presents an additional advantage as excess PLPs can block DO binding sites in the detection step. Both Strategies I and II tolerate a significant surplus of the PLPs as the concentration of target DNA is not known in a real sample.

With the MMB handling, the overall assay performance was similar or better compared to heterogeneous linear RCA assays reported by others [20, 21, 33–35]. Our results indicate that MMB mixing significantly impacts the results and can cause a variation of the obtained signal [25]. It is likely that a higher reproducibility can be obtained when the mixing and sample processing are automated. In perspective, the sensitivity of RCA can be further increased by implementing C2CA [4, 25] in which the first round of amplification takes place on MMBs followed by digestion and a second round of MMB-free PLP ligation and amplification.

Conclusion

We studied and compared strategies for the capture, transportation and selective release of DNA target for an assay based on rolling circle amplification integrated with an optomagnetic readout of the amplification products. The overall assay time, including 45 min of RCA, was in all cases at most 2.5 h.

In a reference assay without microbead sample handling and direct detection of the binding of magnetic nanoparticles to rolling circle amplification products, we found a limit of detection of 200 fM. We implemented a strategy for the selective and irreversible release of rolling circle products from the microbeads during the detection step that facilitated detection of the binding of magnetic nanoparticles with limits of detection of 4-20 pM. In addition, we tested a strategy to first capture magnetic nanoparticles on rolling circle products on microbeads during amplification followed by detection of their subsequent release in a high-pH buffer with a limit of detection of 10 pM obtained with a 2.3 h assay time.

The higher limits of detection found for the assays with microbead sample handling were due to a combination of the increased variability of the results introduced by using the microbeads and the reduced diffusion and reduced polymerase activity when the targets are bound to the solid surface of the microbeads.

The presented DNA-handling strategies are useful for any assay strategies where there is a need for the selective capture, transportation and non-destructive release of a DNA target and are also amenable for integration in robotic sample handling or in lab-on-a-chip systems. Our future work aims to automate the assay handling and implement a mild microbead mixing procedure and to transfer the assay to a lab-on-a-chip platform.

Acknowledgements We thank Mats Nilsson (SciLifeLab, Stockholm) for design of Influenza target and probes as well as for the routine protocols of MMB-free circularization and rolling circle amplification.

Compliance with Ethical Standards

The author(s) declare that they have no competing interests.

References

1. Zhao Y, Chen F, Li Q, Wang L, Fan C (2015) Isothermal amplification of nucleic acids. Chem Rev 115(22):12491–12545
2. Ali MM, Li F, Zhang Z, Zhang K, Kang DK, Ankrum JA, Le XC, Zhao W (2014) Rolling circle amplification: a versatile tool for chemical biology, materials science and medicine. Chem Soc Rev 43:3324–3341
3. Pavankumar AR, Engström A, Liu J, Herthnek D, Nilsson M (2016) Proficient detection of multi-drug-resistant mycobacterium tuberculosis by padlock probes and lateral flow nucleic acid biosensors. Anal Chem 88(8):4277–4284
4. Göransson J, Ke R, Nong RY, Howell WM, Karman A, Grawé J, Stenberg J, Granberg M, Elgh M, Herthnek D, Wikström P, Jarvius J, Nilsson M (2012) Rapid identification of bio-molecules applied for detection of biosecurity agents using rolling circle amplification. PLoS ONE 7:e31068
5. Clausson CM, Arngården L, Ishaq O, Klaesson A, Kühnemund M, Grannas K, Koos B, Qian X, Ranefall P, Krzywkowski T, Brismar H, Nilsson M, Wählby C, Söderberg O (2015) Compaction of rolling circle amplification products increases signal integrity and signal-to-noise ratio. Sci Rep 5(1):12317
6. Nilsson M, Gullberg M, Dahl F, Szuhai K, Raap AK (2002) Real-time monitoring of rolling-circle amplification using a modified molecular beacon design. Nucleic Acids Res 30(14):e66
7. Jarvius J, Meln J, Göransson J, Stenberg J, Fredriksson S, Gonzalez-Rey C, Bertilsson S, Nilsson M (2006) Digital quantification using amplified single-molecule detection. Nat Methods 3:725–727
8. Kühnemund M, Wei Q, Darai E, Wang Y, Iván HN, Yang Z, Tseng D, Ahlford A, Mathot L, Sjöblom T, Ozcan A, Nilsson M (2017) Targeted DNA sequencing and in situ mutation analysis using mobile phone microscopy. Nat Commun 8:13913

9. Strömberg M, Göransson J, Gunnarsson K, Nilsson M, Svedlindh P, Strømme M (2008) Sensitive molecular diagnostics using volume-amplified magnetic nanobeads. Nano Lett 8(3):816–821
10. Donolato M, Antunes P, de la Torre TZG, Hwu ET, Chen CH, Burger R, Rizzi G, Bosco FG, Strømme M, Boisen A, Hansen MF (2015) Quantification of rolling circle amplified DNA using magnetic nanobeads and a Blu-ray optical pick-up unit. Biosensors Bioelectron 67:649–655
11. Mezger A, Fock J, Antunes P, FW Østerberg, Boisen A, Nilsson M, Hansen MF, Ahlford A, Donolato M (2015) Scalable DNA-based magnetic nanoparticle agglutination assay for bacterial detection in patient samples. ACS Nano 9:7374–7382
12. Li J, Deng T, Chu X, Yang R, Jiang J, Shen G, Yu R (2010) Rolling circle amplification combined with gold nanoparticle aggregates for highly sensitive identification of single-nucleotide polymorphisms. Anal Chem 82:2811–16
13. Peyman SA, Iles A, Pamme N (2009) Mobile magnetic particles as solid-supports for rapid surface-based bioanalysis in continuous flow. Lab Chip 9:3110–3117
14. Gijs MA, Lacharme F, Lehmann U (2010) Microfluidic applications of magnetic particles for biological analysis and catalysis. Chem Rev 110:1518–1563
15. Rödiger S, Liebsch C, Schmidt C, Lehmann W, Resch-Genger U, Schedler U, Schierack P (2014) Nucleic acid detection based on the use of microbeads: a review. Microchim Acta 181:1151–1168
16. Van Reenen A, De Jong AM, Den Toonder JM, Prins MW (2014) Integrated lab-on-chip biosensing systems based on magnetic particle actuation-a comprehensive review. Lab Chip 14(12):1966–1986
17. Pandit KR, Nanayakkara IA, Cao W, Raghavan SR, White IM (2015) Capture and direct amplification of DNA on chitosan microparticles in a single PCR-optimal solution. Anal Chem 87:11022–11029
18. Neumann F, Hernández-Neuta I, Grabbe M, Madaboosi N, Albert J, Nilsson M (2018) Padlock probe assay for detection and subtyping of seasonal influenza. Clin Chem 64:e12
19. Palanisamy R, Connolly AR, Trau M (2010) Considerations of solid-phase DNA amplification. ACS Bioconjugate Chem 21:690–695
20. Schopf E, Fischer NO, Chen Y, Tok JB (2008) Sensitive and selective viral DNA detection assay via microbead-based rolling circle amplification. Bioorganic Med Chem Lett 18:5871–5874
21. Sato K, Ishii R, Sasaki N, Sato K, Nilsson M (2013) Bead-based padlock rolling circle amplification for single DNA molecule counting. Anal Biochem 437(1):43–45
22. Sato K, Tachihara A, Renberg B, Mawatari K, Sato K, Tanaka Y, Jarvius J, Nilsson M, Kitamori T (2010) Microbead-based rolling circle amplification in a microchip for sensitive DNA detection. Lab Chip 10:1262–1266
23. Ahlford A, Conde A, Sabourin D, Kutter J, Nilsson M, Dufva M, Brivio M (2011) A microfluidic platform for personalized cancer diagnostics by padlock probes ligation and circle-to-circle amplification. In: 15th International conference on miniaturized systems for chemistry and life sciences 2011 (MicroTAS 2011), pp 61–63
24. Kühnemund M, Witters D, Nilsson M, Lammertyn J (2014) Circle-to-circle amplification on a digital microfluidic chip for amplified single molecule detection. Lab Chip 14:2983
25. Hernández-Neuta I, Pereiro I, Ahlford A, Ferraro D, Zhang Q, Viovy JL, Descroix S, Nilsson M (2018) Microfluidic magnetic fluidized bed for DNA analysis in continuous flow mode. Biosensors Bioelectron 102:531–539
26. Schopf E, Liu Y, Deng JC, Yang S, Cheng G, Chen Y (2011) Mycobacterium tuberculosis detection via rolling circle amplification. Anal Methods 3:267–273
27. Minero GAS, Nogueira C, Rizzi G, Tian B, Fock J, Donolato M, Strömberg M, Hansen MF (2017) Sequence-specific validation of LAMP amplicons in real-time optomagnetic detection of Dengue serotype 2 synthetic DNA. Analyst 142:3441–3450
28. Fock J, Balceris C, Costo R, Zeng L, Ludwig F, Hansen MF (2017) Field-dependent dynamic responses from dilute magnetic nanoparticle dispersions. Nanoscale 10:2052–2066
29. Strömberg M, Zardán Gómez de la Torre T, Göransson J, Gunnarsson K, Nilsson M, Strømme M, Svedlindh P (2008) Microscopic mechanisms influencing the volume amplified magnetic nanobead detection assay. Biosensors Bioelectron 24:696–703
30. Strömberg M, Zardán Gómez De La Torre T, Göransson J, Gunnarsson K, Nilsson M, Svedlindh P, Strømme M (2009) Multiplex detection of DNA sequences using the volume-amplified magnetic nanobead detection assay. Anal Chem 81:3398–3406
31. Zardán Gómez De La Torre T, Strömberg M, Russell C, Göransson J, Nilsson M, Svedlindh P, Strømme M (2010) Investigation of immobilization of functionalized magnetic nanobeads in rolling circle amplified DNA coils. J Phys Chem B 114:3707–3713
32. Oishi M (2015) Enzyme-free and isothermal detection of microRNA based on click-chemical ligation-assisted hybridization coupled with hybridization chain reaction signal amplification. Anal Bioanal Chem 407(14):4165–72
33. Zhang S, Wu Z, Shen G, Yu R (2009) A label-free strategy for SNP detection with high fidelity and sensitivity based on ligation-rolling circle amplification and intercalating of methylene blue. Biosensors Bioelectron 24:3201–3207
34. Schopf E, Chen Y (2010) Attomole DNA detection assay via rolling circle amplification and single molecule detection. Anal Biochem 397:115–117
35. Yang X, Yang K, Zhao X, Lin Z, Liu Z, Luo S, Zhang Y, Wang Y, Fu W (2017) Terahertz spectroscopy for the isothermal detection of bacterial DNA by magnetic bead-based rolling circle amplification. Analyst 142(24):4661–4669